NMR studies of structure and ferroelectricity for Rochelle salt nanoparticles embedded in mesoporous sieves

2008 J. Phys.: Condens. Matter 20 215205

(http://iopscience.iop.org/0953-8984/20/21/215205)

J. Phys.: Condens. Matter **20** (2008) 215205 (6pp) doi:10.1088/0953-8984/20/21/215205

NMR studies of structure and ferroelectricity for Rochelle salt nanoparticles embedded in mesoporous sieves

Cheng Tien[1,2], E V Charnaya[1,3,6], M K Lee[1], S V Baryshnikov[4], D Michel[5] and W Böhlmann[5]

[1] Department of Physics, National Cheng Kung University, Tainan 70101, Taiwan, Republic of China
[2] Center for Micro/Nano Science of Technology, National Cheng Kung University, Tainan 70101, Taiwan, Republic of China
[3] Institute of Physics, St Petersburg State University, St Petersburg, Petrodvorets, 198504, Russia
[4] Blagoveschensk State Pedagogical University, Blagoveschensk, 675002, Russia
[5] Faculty of Physics and Geosciences, University of Leipzig, Leipzig, D-04103, Germany

E-mail: charnaya@live.com

Received 10 January 2008, in final form 25 February 2008
Published 18 April 2008
Online at stacks.iop.org/JPhysCM/20/215205

Abstract
NMR studies were carried out for Rochelle salt embedded in molecular sieves. ^{23}Na magic angle spinning (MAS) and multiple quantum (MQ) MAS NMR spectra revealed a complex structure of the confined crystalline material. The major part of particles within nanopores had a structure similar to that of bulk Rochelle salt. The ^{23}Na spin–lattice relaxation times at various temperatures associated with this modification were also similar to those for bulk Rochelle salt and showed broad minima that corresponded to the ferroelectric and re-entrant phase transitions under nanoconfinement at temperatures just below the relevant transitions in bulk. This result suggests that the bulk-like modification within pores is ferroelectric in between. Fast spin relaxation in the rest of the confined material reflected high molecular mobility.

1. Introduction

The structure and physical properties of materials embedded in solid nanoporous matrices have recently attracted a great deal of attention. Filled porous matrices are considered as prospective nanocomposites for technical applications. The dimensions and arrangement of confined particles are mainly governed by the geometry of the pore network. This gives rise to the possibility to create arrays of small particles of certain sizes and interparticle distances. Because of the small pore diameters, the properties of confined materials are expected to be influenced by various size effects. Therefore, studies of such nanocomposites provide information about size effects in large assemblies of small particles.

Porous matrices filled with liquid crystals, simple and organic liquids, metals, superionics, and polymers have all been studied (see [1–7] and references therein). The melting and freezing phase transitions, glass formation, atomic and molecular diffusion, crystalline lattice symmetry, superconductivity, and phase transformations in liquid crystals were found to be affected by nanoconfinement.

Studies of ferroelectricity in confined geometry are comparatively poor. It has been reported lately that sodium nitrite nanocrystalline particles have been embedded in artificial opals, porous glasses, and molecular sieves [8–13], Rochelle salt was introduced into porous alumina [14], and some other ferroelectric particles into porous glasses [13, 15]. Ferroelectricity was studied mainly for confined sodium nitrite [8, 10, 13, 15–17]. The ferroelectric phase transition in confined sodium nitrite was found to occur close to the critical

[6] Author to whom any correspondence should be addressed.

point in bulk $NaNO_2$ [8, 10, 12, 13]. In contrast, the upper ferroelectric transition in Rochelle salt within porous alumina was reported to move drastically to high temperature [14]. The fabrication of opal photonic crystals infiltrated with barium, strontium, and lead titanate was reported in [18, 19], but ferroelectric properties for those composites were not studied.

In the present paper we report results of NMR studies of Rochelle salt small particles confined within the molecular sieves MCM-41 and SBA-15. Bulk Rochelle salt, $NaKC_4H_4O_6{\cdot}4H_2O$, was the first ferroelectric discovered. It exhibits ferroelectricity at room temperature and undergoes two second-order phase transitions into paraelectric states of the identical structure upon warming at 297 K and upon cooling at 255 K [20].

As far as we know, the only studies of Rochelle salt under confinement were made for Rochelle salt embedded in porous alumina [14]. The spontaneous polarization was measured and found to exist in the range from room temperature to the melting point which is noticeably higher than the upper ferroelectric phase transition temperature in bulk. The channel sizes (average diameter of about 30 nm) and distance between channels in porous alumina used in [14] were much larger than in the MCM-41 and SBA-15 molecular sieves. Therefore one can expect the behavior of Rochelle salt embedded in the molecular sieves to differ from that of the same material within porous alumina. Two main points have to be dealt with. The first is whether a regular crystalline structure can form within molecular sieves and whether it is similar to that in bulk Rochelle salt. This point is of particular importance since the parameters of the Rochelle salt unit cell are of the same order of magnitude as the pore size for molecular sieves. The second point is whether Rochelle salt embedded in molecular sieves undergoes phase transitions and what their temperatures are under confinement.

NMR has already proved to be a very powerful tool for investigations of particles under nanoconfinement due to its high sensitivity to local environments and lattice dynamics. In the present paper we will show that the major part of Rochelle salt embedded in nanopores has a crystalline structure similar to that in bulk which is evidenced by bulk-like ^{23}Na MAS NMR spectra and spin–lattice relaxation. It also exhibits diffuse spin relaxation anomalies corresponding to the ferroelectric and re-entrant phase transitions at temperatures slightly below the relevant transitions in bulk. Another minor part of confined material has a distinctive structure and spin relaxation associated with high molecular mobility.

2. Experiment and samples

MCM-41 and SBA-15 molecular sieves were used as nanoporous matrices. They have an ordered honeycomb structure of cylindrical pores with amorphous silica walls [21, 22]. The MCM-41 molecular sieves were synthesized following [21, 23] with typical pore sizes of 37, 26, and 20 Å found from electron microscopy and nitrogen adsorption–desorption isotherms. The synthesis of SBA-15 was performed using a method described in [22]. The pore size estimated from nitrogen adsorption–desorption isotherms was 52 Å.

Rochelle salt was embedded in MCM-41 and SBA-15 from aqueous solution. The molecular sieve powder was put in such an amount of the Rochelle salt saturated solution that all the liquid penetrated into pores. Then the powder was dried and pressed into pellets. The residual solution fraction was negligibly small since NMR measurements did not reveal narrow lines which could be associated with liquid. The room temperature x-ray powder diffraction patterns showed only very weak narrow lines corresponding to the most pronounced peaks for bulk Rochelle salt crystallized on the outer surface of molecular sieves. The estimated amount of bulk compound was very small compared to the total amount of Rochelle salt used to produce the samples and expected from the intensity of NMR signals, and therefore could not influence noticeably the experimental results. No reliable broadened peaks associated with small particles were observed. Assuming that most Rochelle salt is confined within pores, the pore filling factor was estimated as 0.7 by weighing the samples before and after filling.

^{23}Na (spin $I = 3/2$) NMR measurements for confined Rochelle salt were carried out using Bruker Avance400 and Avance750 NMR pulse spectrometers operating at a Larmor frequency of 105.8 MHz (at magnetic field 9.4 T) and 198.3 MHz (at magnetic field 17.6 T), respectively. The ^{23}Na magic angle spinning (MAS) NMR spectra were obtained at 300 K, above the upper phase transition point of bulk Rochelle salt. The typical 90° pulse was 1.9 and 1.7 μs at lower and higher magnetic fields, respectively. The ^{23}Na multiple quantum (MQ) MAS NMR [24, 25] measurements were carried out at 296 K and field 9.4 T using a three-pulse sequence for the Rochelle salt loaded MCM-41 molecular sieves with 37 and 20 Å pores. The spinning rate was 12 kHz. The static ^{23}Na NMR spectra and longitudinal spin relaxation were measured near room temperature for all samples under study and within a range from about 240 to 315 K for Rochelle salt loaded MCM-41 with 26 Å pore size using the Avance400 spectrometer. The latter temperature range covers both Curie points in bulk. Measurements of longitudinal magnetization recovery were carried out starting from 280 K, far from the ferroelectric phase transitions in bulk Rochelle salt. Then the sample was cooled down or warmed up to 240 or 315 K, respectively. Accuracy of temperature stabilization during measurements was better than 0.2 K. The longitudinal magnetization recovery was observed with the inversion–recovery technique. The 90° pulse was 1.95 μs. All spectra were referenced to the ^{23}Na NMR signal in NaCl 1 M aqueous solution at room temperature. Similar studies were performed for powder Rochelle salt.

3. Experimental results

The central bands of the ^{23}Na MAS spectra at 300 K at the field 17.6 T for bulk powder Rochelle salt and filled MCM-41 molecular sieves with the 20 Å pore size are shown in figures 1(a) and (b), respectively. The central band for Rochelle salt confined within 26 Å pores at the field 9.4 T is shown in the inset to figure 1. Central bands very similar to those shown in figure 1(b) and the inset were also obtained for molecular

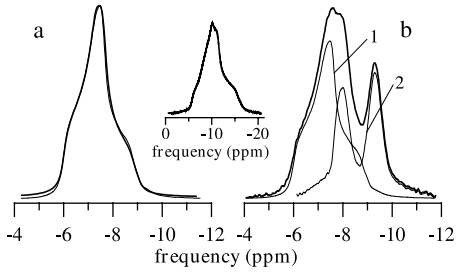

Figure 1. Experimental ^{23}Na MAS NMR central bands obtained at magnetic field 17.6 T for bulk (a) and confined within 20 Å pores (b) Rochelle salt (thick lines). The thin line in (a) shows the simulated central band. In (b) the thin lines show the deconvolution of the experimental band: (1) is the central band with bulk-like parameters, (2) is the complement to the experimental central band. The inset shows the experimental ^{23}Na MAS NMR central band for Rochelle salt confined within 26 Å pores at magnetic field 9.4 T.

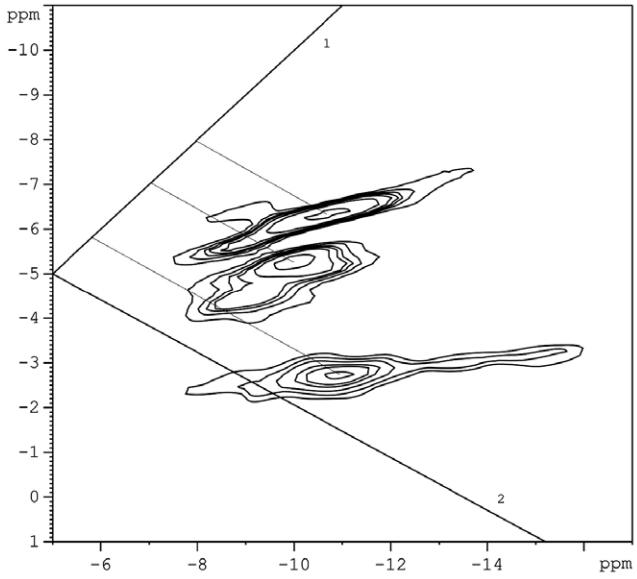

Figure 2. ^{23}Na MQ MAS spectrum for the sample with 37 Å pores. 1 is the chemical shift axis, 2 is the quadrupolar induced shift axis. The subsidiary straight lines are drawn to allow reading the isotropic chemical shift as described in the text.

sieves with other pore sizes. They are mainly caused by $+1/2 \leftrightarrow -1/2$ transitions and are broadened by the second-order quadrupole interactions [26].

The total ^{23}Na MAS spectra for bulk and confined Rochelle salt were expanded over large frequency ranges in agreement with broad central bands and were quite similar. However, sidebands for confined Rochelle salt were split and had a low frequency shoulder revealing an additional set of lines. The splitting of sidebands was seen within a frequency range about half as large as for the primary spectra.

The central part of the two-dimensional MQ MAS spectrum obtained after shearing Fourier transformation for the sample with 37 Å pores is shown in figure 2. In this figure, the anisotropy axis is directed horizontally and a projection of the 2D spectrum onto the vertical axis displays only isotropic shifts, while the second-order quadrupolar broadened ridges

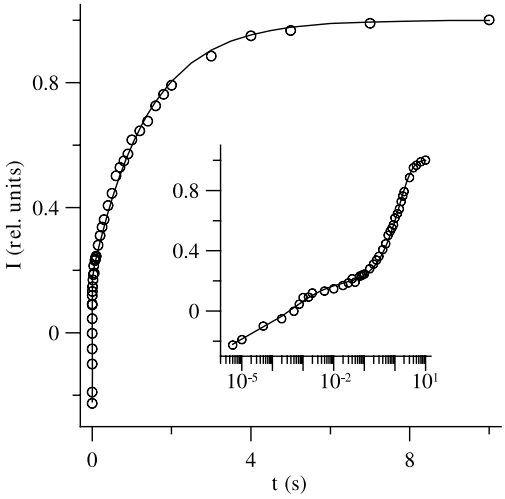

Figure 3. Dependence of the integral intensity I of the static NMR signal on the time t between π and $\pi/2$ pulses for the Rochelle salt loaded MCM-41 with 26 Å pores at 294 K. The solid line is a fit using relationship (1) and parameters $b = 0.61$, $T_{1s} = 1.41$ s, $T_{1f} = 0.3$ ms, $\alpha = 0.3$, and $b = 1.34$. The inset shows the same dependence on the semi-logarithmic scale, to make clear the fit at short times t.

appear parallel to the horizontal axis. One can clearly see three distinctive peaks corresponding to different sodium sites. A similar 2D spectrum was obtained for the sample with 20 Å pores. The MQ MAS spectrum for bulk Rochelle salt shows only one peak corresponding to the lowest one in figure 2.

Static ^{23}Na spectra for confined as well as for bulk powder Rochelle salt consisted of a single line corresponding chiefly to the central $+1/2 \leftrightarrow -1/2$ transitions. The recovery of this line after an inversion pulse occurred for confined Rochelle salt in two distinct steps at all temperatures in contrast to single-exponential relaxation in bulk [27, 28]. An example for the sample with 26 Å pores at $T = 294$ K is shown in figure 3. The relaxation rates at the initial and second steps differ remarkably (figure 3). Because of the pronounced difference in relaxation rate for the two steps, the longitudinal magnetization recovery can be uniquely divided into two relaxation processes, slow and fast. The total recovery curves at various temperatures were well fitted by a sum of single and stretched exponentials (see figure 3)

$$I(t) = 1 - a[b\exp(-t/T_{1s}) + (1-b)\exp(-t/T_{1f})^{\alpha}], \quad (1)$$

where $I(t)$ is the normalized longitudinal nuclear magnetization at time t; $1-a$ is the intensity of the NMR signal immediately after magnetization inversion; T_{1s} and T_{1f} are relaxation times corresponding to slow and fast components, respectively; b is the proportion of the slow component; α is the stretched exponent for the fast component.

The proportion b of the slow component for particular samples did not change noticeably with temperature and was equal to about 0.60 and 0.61 for 20 and 26 Å pore sizes, respectively, and to 0.65 for 37 and 52 Å pores. The temperature dependence of T_{1s} for Rochelle salt embedded in 26 Å pores is shown in figure 4 for several different

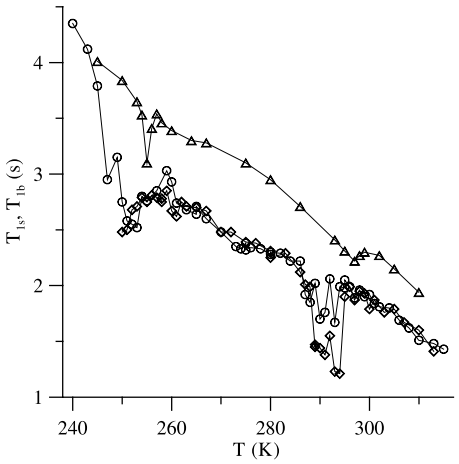

Figure 4. ^{23}Na spin relaxation times T_{1s} for Rochelle salt embedded in MCM-41 with 26 Å pores (circles and diamonds) and T_{1b} in bulk Rochelle salt (triangles) at various temperatures at magnetic field 9.4 T. Solid lines are guides for the eye.

runs started at 280 K. The stretched exponent α at different temperatures lay between 0.3 and 0.35. The relaxation time T_{1f} continuously increased with decreasing temperature from about 0.3 to 2 ms. Results for spin–lattice relaxation were also obtained for bulk powder Rochelle salt for comparison. Since the magnetization recovery in the bulk was single exponential, it can be defined by a spin–lattice relaxation time T_{1b} whose temperature dependence is shown in figure 4.

4. Discussion

Bulk Rochelle salt is monoclinic (space group $P2_1$) in the ferroelectric phase and orthorhombic (space group $P2_12_12$) in the low and high temperature paraelectric phases with four molecules in a unit cell (see, for instance, [29, 30]). The orthorhombic unit cell parameters near the upper phase transition are equal to $a = 11.9$, $b = 14.3$, $c = 6.2$ Å. Because of the low symmetry of the crystalline lattice, the static gradients of the electric field at sodium sites are not zero and act on the nuclear quadrupole moments. The ^{23}Na quadrupole coupling was studied using static NMR in single-crystalline Rochelle salt in [31–34]. The quadrupole coupling constant $C_q = e^2qQ/h$ and asymmetry parameter $\eta = (V_{yy} - V_{xx})/V_{zz}$ were evaluated for the paraelectric and ferroelectric phases. Here, V_{ii} are components of the electric field gradient tensor (on principal axes) at ^{23}Na sites, e is the electron charge, Q is the ^{23}Na quadrupole moment, $eq \equiv V_{zz}$, h is the Planck constant. Above the upper phase transition at 303 K, $C_q = 1.313$ MHz and $\eta = 0.809$ for all four sodium ions in a unit cell [31]. In the ferroelectric phase two sublattices are formed in agreement with the crystalline symmetry. They have different ^{23}Na quadrupole parameters; however, even in the middle of the ferroelectric phase at 273 K the difference between the quadrupole constants of the sublattices is not large (1.407 and 1.285 MHz [31, 32]). In the lower paraelectric phase the four sodium sites are in equivalent environments again with the quadrupole constant $C_q = 1.363$ MHz at 248 K [33]. As far as we know, no ^{23}Na MAS NMR studies of bulk Rochelle salt have been performed previously.

The MAS central band shape for bulk Rochelle salt at 300 K was fitted using the Dmfit program [35] (figure 1(a)). The fitting parameters were $C_q = 1.313$ MHz, $\eta = 0.82$, and the isotropic shift $\delta = -5.9$ ppm. The values of C_q and η lie quite close to those found for single-crystalline Rochelle salt in the upper paraelectric phase. The total MAS spectra agree with these quadrupole parameters while the central band simulation provides much better accuracy.

The ^{23}Na central bands for confined Rochelle salt obtained at 17.6 T are structured (figure 1(b)). They can be fitted as the convolution of a bulk-like line and a complex line with two maxima as shown in figure 1(b). The parameters C_q, η, and δ for the former were assumed the same as for bulk Rochelle salt. This agrees with the total MAS spectra for confined Rochelle salt which were similar to that for bulk. The bulk-like and additional lines are not resolved at lower field (figure 1, inset) when the second-order quadrupole coupling is stronger [26]. This evidences the magnetic origin of the fine structure of the additional complex line at 17.6 T.

The MQ MAS spectra agree with the deconvolution of the MAS central bands and provide information on the number of different sodium sites, their chemical shifts and quadrupole coupling. To find the isotropic chemical shift δ_{Ch} one should draw a line parallel to the quadrupolar induced shift axis (axis 2 in figure 2) from the top of peaks to the crossing with the chemical shift axis (axis 1 in figure 2). The ordinate of the crossing point gives δ_{Ch} while the ordinate of the top of peaks gives the sum δ_G of the isotropic chemical shift and quadrupolar induced shift. The lowest ridge in figure 2 corresponds to the bulk-like Rochelle salt within nanopores with $\delta_{Ch} \cong -5.9$ ppm. Two other peaks have isotropic chemical shifts equal to about -7 and -8 ppm and noticeably weaker quadrupole coupling. They can arise due to two additional crystalline modifications in confinement or to two different sodium sites in one modification.

The results obtained showed a composite structure of particles within pores. The main part of Rochelle salt under nanoconfinement forms bulk-like crystalline lattice. Therefore, one can suggest that ^{23}Na spin–lattice relaxation in this part of confined Rochelle salt should be also similar to that in bulk. Figure 4 shows that the relaxation time T_{1s} associated with the slow component of spin relaxation in confined Rochelle salt lies quite close to the relaxation time T_{1b} in bulk. To get more information about the nature of the slow and fast components of ^{23}Na spin relaxation and to correlate them with the complex MAS lineshapes, we also carried out relaxation measurements under MAS conditions at 300 K and field 17.6 T. Such measurements confirmed that the slow and fast components of relaxation correspond to the recovery of the bulk-like and additional components of the central band, respectively. This can be seen from figure 5 which shows the central band for the sample with 37 Å pores in several stages of recovery after inversion. The time T_{1s} should be mainly caused by reorientations of crystalline water molecules, as in bulk [27, 36].

Times T_{1f} associated with the rest of the confined Rochelle salt are very short. Such short times in non-metallic

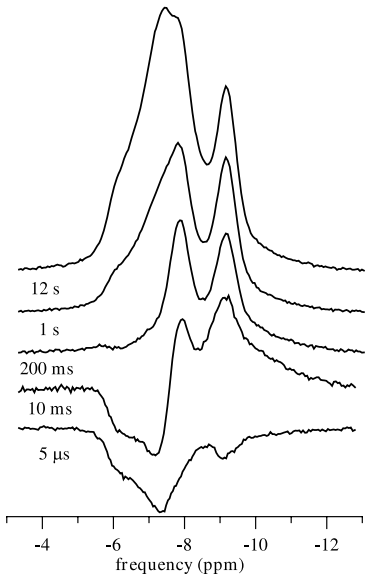

Figure 5. The ^{23}Na MAS NMR central band in different stages of recovery after inversion at magnetic field 17.6 T for Rochelle salt confined within 37 Å pores. The time delays after a 180° pulse are shown in the plot.

compounds are normally observed in the presence of high molecular or atomic mobility, for instance, in solids with fast rotational diffusion of molecular groups. In the particular case of the Rochelle salt loaded molecular sieves T_{1f} can occur due to rapid reorientations of crystalline water molecules. The pronounced departure of the stretched exponent α from 1 evidences a high level of disorder in this part of confined material.

The temperature dependence of T_{1s} for confined Rochelle salt shows regular increase upon decreasing temperature with noticeable deviations against the background below 255 K and just near room temperature (figure 4). Similar behavior was found in bulk powder (figure 4 and [28]) and single-crystalline Rochelle salt [27].

Regular reduction of spin–lattice relaxation with decreasing temperature corresponds to quadrupole relaxation driven by the thermally activated mobility of water molecules [27, 36]. The spin relaxation time dips on approaching the phase transitions in bulk Rochelle salt [27, 28] and deuterated ammonium Rochelle salt [36] were treated as an additional contribution to relaxation caused by critical dynamics of fluctuations [37, 38]. For the order–disorder phase transitions it is related to the slowdown of the order parameter relaxation time. Theoretical treatments of dynamics in bulk Rochelle salt performed in [39, 40] showed that it exhibited two-mode relaxational behavior; the correlation time of one of the two modes slows down on approaching the two Curie points in agreement with dielectric and acoustic data. In the case of anisotropic dipole interactions the spin–lattice relaxation time should decrease near the transition according to $1/\ln|(T - T_c)|$ [37]. Therefore, the critical anomalies of nuclear spin relaxation can be used as indicators of the phase transitions. Such indicators are especially suitable for detecting phase transitions in confined geometry.

Figure 4 evidences two pronounced T_{1s} dips at about 250 and 290 K. They are slightly shifted to low temperature compared to the relevant critical anomalies for bulk Rochelle salt and are strongly broadened. This result confirms that the upper ferroelectric and lower re-entrant phase transitions in confined Rochelle salt occur slightly below the Curie points in bulk while they are noticeably diffused. Thus one can suggest that the main part of Rochelle salt within pores is in the ferroelectric state in between.

Smearing of the phase transitions for Rochelle salt within nanopores can be related to some distribution of the Curie points among different confined particles caused by heterogeneity in the particle size and shape. There is an analogy here with diffused phase transitions in doped or irradiated ferroelectric crystals (see, for instance, [41]). The decrease in the phase transition temperature can arise due to small particle sizes and, consequently, to the increased surface-to-volume ratio. Recently, a phenomenological model based on the Landau free energy expansion was developed to treat size effects on the ferroelectric phase transitions in small spherical and cylindrical particles (see [42, 43] and references therein). It was found for particles in non-polarized environments that the phase transition temperature should shift deeper into the ferroelectric state upon decreasing the particle size. Therefore, this approach can provide an explanation for the reduction of the upper ferroelectric phase transition temperature in confined Rochelle salt, but it does not explain the shift of the re-entrant phase transition to low temperature. Probably, size effects on phase transitions in a ferroelectric with two polarized sublattices require special consideration.

In conclusion, ^{23}Na NMR studies of Rochelle salt embedded in pores of the MCM-41 and SBA-15 molecular sieves have shown that the confined material forms a complex crystalline structure. The major confined crystalline modification is similar to that of bulk Rochelle salt. Nuclear spin–lattice relaxation in this modification shows a temperature dependence which reveals two structural phase transitions as in bulk, but broadened and slightly shifted to low temperature. This result evidences that the major part of embedded Rochelle salt is ferroelectric between these two transitions. The rest of the confined material exhibits fast spin relaxation associated with high molecular mobility.

Acknowledgments

The present work was supported by Taiwan government under Grant OUA 95-21T-2-017, by RFBR (Russia) and by DFG (Germany).

References

[1] Kärger J and Ruthven D M 1992 *Diffusion in Zeolites and Other Microporous Solids* (New York: Wiley)
[2] Crawford G P and Zumer S (ed) 1996 *Liquid Crystals in Complex Geometries* (London: Taylor and Francis)
[3] Alcoutlabi M and McKenna G B 2005 *J. Phys.: Condens. Matter* **17** R461
[4] Christenson H K 2001 *J. Phys.: Condens. Matter* **13** R95
[5] Lopez C 2003 *Adv. Mater.* **15** 1679

[6] Charnaya E V, Tien C, Lin K J, Kumzerov Yu A and Wur C-S 1998 *Phys. Rev.* B **58** 467
[7] Tien C, Wur C S, Lin K J, Charnaya E V and Kumzerov Yu A 2000 *Phys. Rev.* B **61** 14833
[8] Pankova S V, Poborchii V V and Solovev V G 1996 *J. Phys.: Condens. Matter* **8** L203
[9] Fokin A V, Kumzerov Yu A, Okuneva N M, Naberezhnov A A, Vakhrushev S B, Golosovsky I V and Kurbakov A I 2002 *Phys. Rev. Lett.* **89** 175503
[10] Tien C, Charnaya E V, Lee M K, Baryshnikov S V, Sun S Y, Michel D and Böhlmann W 2005 *Phys. Rev.* B **72** 104105
[11] Murzina T V, Sychev F Y, Kolmychek I A and Aktsiperov O A 2007 *Appl. Phys. Lett.* **90** 161120
[12] Kutnjak Z, Vodopivec B, Blinc R, Fokin A V, Kumzerov Y A and Vakhrushev S B 2005 *J. Chem. Phys.* **123** 084708
[13] Rysiakewicz-Pasek E, Poprawski R, Polanska J, Urbanowicz A and Sieradzki A 2006 *J. Non-Cryst. Solids* **352** 4309
[14] Yadlovker D and Berger S 2005 *Phys. Rev.* B **71** 184112
[15] Colla E V, Fokin A V, Koroleva E Yu, Kumzerov Yu A, Vakhrushev S B and Savenko B N 1999 *Nanostruct. Mater.* **12** 963
[16] Baryshnikov S V, Charnaya E V, Tien C, Michel D, Andriyanova N P and Stukova E V 2007 *Phys. Solid State* **49** 791
[17] Baryshnikov S V, Stukova E V, Charnaya E V, Tien C, Lee M K, Böhlmann W and Michel D 2006 *Phys. Solid State* **48** 593
[18] Zhou J, Sun C Q, Pita K, Lam Y L, Zhou Y, Ng S L, Kam C H, Li L T and Gui Z L 2001 *Appl. Phys. Lett.* **78** 661
[19] Kim B G, Parikh K S, Ussery G, Zakhidov A, Baughman R H, Yablonovitch E and Dunn B S 2002 *Appl. Phys. Lett.* **81** 4440
[20] Lines M E and Glass A M 2001 *Principles and Applications of Ferroelectrics and Related Materials* (Oxford: Clarendon)
[21] Kresge C T, Leonowicz M E, Roth W J, Vartuli J C and Beck J S 1992 *Nature* **359** 710
[22] Jun S, Joo S H, Ryoo R, Kruk M, Jaroniec M, Liu Z, Ohsuma T and Terasaki O 2000 *J. Am. Chem. Soc.* **122** 10712
[23] Böhlmann W and Michel D 2001 *Stud. Surf. Sci. Catal.* **135** 202
[24] Frydman L and Harwood J S 1995 *J. Am. Chem. Soc.* **117** 5367
[25] Fernandez C and Amoureux J P 1995 *Chem. Phys. Lett.* **242** 449
[26] Abragam A 1989 *Principles of Nuclear Magnetism* (Oxford: Clarendon)
[27] Bonera G, Borsa F and Rigamonti A 1969 *Phys. Lett.* A **29** 88
[28] Tien C, Charnaya E V, Lee M K and Baryshnikov S V 2007 *Phys. Solid State* **49** 1326
[29] Shiozaki Y, Shimizu K and Nozaki R 2001 *Ferroelectrics* **261** 239
[30] Solans X, Gonzalez-Silgo C and Ruiz-Pérez C 1997 *J. Solid State Chem.* **131** 350
[31] Miller N C and Casabella P A 1966 *Phys. Rev.* **152** 228
[32] Fitzgerald M E and Casabella P A 1973 *Phys. Rev.* B **7** 2193
[33] Fitzgerald M E and Casabella P A 1970 *Phys. Rev.* B **2** 1350
[34] Blinc R, Petkovšek J and Zupančič I 1964 *Phys. Rev.* **136** A1684
[35] Massiot D, Fayon F, Caprou M, King I, Le Calve S, Alonso B, Durand J-D, Bujoli B, Gan Z and Hoatson G 2002 *Magn. Reson. Chem.* **40** 70
[36] Apih T, Dolinšek J, Topič B, Blinc R and Shuvalov L A 1990 *Phys. Rev.* B **41** 7227
[37] Bonera G, Borsa F and Rigamonti A 1970 *Phys. Rev.* B **2** 2784
[38] Blinc R and Zimer S 1968 *Phys. Rev. Lett.* **21** 1004
[39] Kulda J, Hlinka J, Kamba S and Petzelt J *ILL: Annual Report 2000* www.ill.fr/AR-00/p-48.htm
[40] Žekš B, Shukla G C and Blinc R 1971 *Phys. Rev.* B **3** 2306
[41] Charnaya E V and Rakhimov I 1990 *Ferroelectrics* **112** 45
[42] Zhong W L, Wang Y G, Zhang P L and Qu B D 1994 *Phys. Rev.* B **50** 698
[43] Wang C L, Xin Y, Wang X S and Zhong W L 2000 *Phys. Rev.* B **62** 11423